J|A|C|S
ARTICLES
Published on Web 04/05/2002

Spectroscopic Studies of 1-Aminocyclopropane-1-carboxylic Acid Oxidase: Molecular Mechanism and CO_2 Activation in the Biosynthesis of Ethylene

Jing Zhou,[†] Amy M. Rocklin,[‡] John D. Lipscomb,*[,‡] Lawrence Que, Jr.,*[,‡] and Edward I. Solomon*[,†]

Contribution from the Department of Chemistry, Stanford University, Stanford, California 94305, and the Departments of Chemistry and Biochemistry, Molecular Biology and Biophysics and the Center for Metals in Biocatalysis, University of Minnesota, Minneapolis, Minnesota 55455

Received October 5, 2001

Abstract: 1-Aminocyclopropane-1-carboxylic acid (ACC) oxidase (ACCO) catalyzes the last step in the biosynthesis of the gaseous plant hormone ethylene, which is involved in development, including germination, fruit ripening, and senescence. ACCO is a mononuclear non-heme ferrous enzyme that couples the oxidation of the cosubstrate ascorbate to the oxidation of substrate ACC by dioxygen. In addition to substrate and cosubstrate, ACCO requires the activator CO_2 for continuous turnover. NIR circular dichroism and magnetic circular dichroism spectroscopies have been used to probe the geometric and electronic structure of the ferrous active site in ACCO to obtain molecular-level insight into its catalytic mechanism. Resting ACCO/Fe^{II} is coordinatively saturated (six-coordinate). In the presence of CO_2, one ferrous ligand is displaced to yield a five-coordinate site only when both the substrate ACC and cosubstrate ascorbate are bound to the enzyme. The open coordination position allows rapid O_2 activation for the oxidation of both substrates. In the absence of CO_2, ACC binding alone converts the site to five-coordinate, which would react with O_2 in the absence of ascorbate and quickly deactivate the enzyme. These studies show that ACCO employs a general strategy similar to other non-heme iron enzymes in terms of opening iron coordination sites at the appropriate time in the reaction cycle and define the role of CO_2 as stabilizing the six-coordinate ACCO/Fe^{II}/ACC complex, thus preventing the uncoupled reaction that inactivates the enzyme.

Introduction

1-Aminocyclopropane-1-carboxylic acid (ACC) oxidase (ACCO) catalyzes the last step in the biosynthesis of the gaseous plant hormone ethylene, which is involved in development, including germination, fruit ripening, and senescence.[1,2] ACCO requires the cosubstrate ascorbate and the activator CO_2. ACCO is related to the α-ketoglutarate (α-KG)-dependent subclass of mononuclear non-heme iron enzymes. Most members of this subclass couple the reaction of the oxidative decarboxylation of α-KG to substrate oxidation (hydroxylation, desaturation, oxidative ring-closure, or expansion). ACCO and isopencillin N synthase (IPNS) have sequence homology to these enzymes but do not require α-KG as a cosubstrate. IPNS catalyzes the four-electron oxidation of substrate δ-(L-α-aminoadipoyl)-L-cysteinyl-D-valine (ACV) to isopenicillin N.[3] ACCO requires ascorbate as a cosubstrate and catalyzes the coupled oxidation of ACC and ascorbate to ethylene, HCN, CO_2, and dehydroascorbate, using a single non-heme Fe^{II} ion and dioxygen.[4,5]

There is extensive amino acid sequence homology among some α-KG-dependent enzymes, ACCO, and IPNS.[6−8] X-ray crystal structures are available for IPNS[6,9] and two α-KG-dependent enzymes, deacetoxycephalosporin C synthase (DAOCS)[10] and clavaminate synthase 1 (CS1).[11] These three enzymes share a conserved jelly roll β-barrel core, which contains the conserved Fe^{II} binding residues, namely, a 2His-1Asp(Glu) facial triad.[12] Site-directed mutagenesis studies on ACCO in a number of systems are consistent with the sequence alignment and demonstrate that ACCO also uses the same ligands to bind the Fe^{II} ion.[13] CO_2 was found to be a necessary

* Corresponding author. E-mail: Edward.Solomon@stanford.edu.
[†] Stanford University.
[‡] University of Minnesota.

(1) John, P. *Physiol. Plant.* **1997**, *100*, 583−592.
(2) Prescott, A. G. *J. Exp. Bot.* **1993**, *44*, 849−861.
(3) Baldwin, J. E.; Bradley, M. *Chem. Rev.* **1990**, *90*, 1079−1088.
(4) Adams, D. O.; Yang, S. F. *Proc. Natl. Acad. Sci. U.S.A* **1979**, *76*, 170−174.
(5) Dong, J. G.; Fernandez-Maculet, J. C.; Yang, S. F. *Proc. Natl. Acad. Sci. U.S.A.* **1992**, *89*, 9789−9793.
(6) Roach, P. L.; Clifton, I. J.; Fülöp, V.; Harlos, K.; Barton, G. J.; Hajdu, J.; Andersson, I.; Schofield, C. J.; Baldwin, J. E. *Nature* **1995**, *375*, 700−704.
(7) Borovok, I.; Landman, O.; Kreisberg-Zakarin, R.; Aharonowitz, Y.; Cohen, G. *Biochemistry* **1996**, *35*, 1981−1987.
(8) Tan, D. S. H.; Sim, T.-S. *J. Mol. Biol.* **1996**, *271*, 889−894.
(9) Roach, P. L.; Clifton, I. J.; Hensgens, C. M. H.; Shibata, N.; Schofield, C. J.; Hajdu, J.; Baldwin, J. E. *Nature* **1997**, *387*, 827−830.
(10) Valegård, K.; Vanscheltinga, A. C. T.; Lloyd, M. D.; Hara, T.; Ramaswamy, S.; Perrakis, A.; Thompson, A.; Lee, H. J.; Baldwin, J. E.; Schofield, C. J.; Hajdu, J.; Andersson, I. *Nature* **1998**, *394*, 805−809.
(11) Zhang, Z. H.; Ren, J. S.; Stammers, D. K.; Baldwin, J. E.; Harlos, K.; Schofield, C. J. *Nat. Struct. Biol.* **2000**, *7*, 127−133.
(12) Hegg, E. L.; Que, L. *Eur. J. Biochem.* **1997**, *250*, 625−629.

10.1021/ja017250f CCC: $22.00

activator for ACCO reactivity both in vivo and in vitro.[14,15] CO_2 increases V_{max} more than 10-fold and increases the K_m toward ACC, ascorbate, and dioxygen several-fold.[16−18] Deactivation studies under various conditions show that CO_2 plays a major role in protecting the enzyme from deactivation.[19,20] However, the mechanism by which CO_2 activates ACC oxidase at a molecular level is unknown.[1] While it has been proposed that a lysine residue is involved in CO_2 activation of ACCO,[16] recent site-directed mutagenesis studies have raised doubts about this possibility.[21]

Previously proposed mechanisms of ACCO involved direct binding of ascorbate to the iron before O_2 binding as part of the oxygen activation process.[13,22] EPR and ENDOR studies of NO complexes of ACCO suggested a different mechanism for ACCO,[23] in which the substrate ACC binds in a bidentate mode through its carboxylate and amino group. Activation of dioxygen at the iron center was suggested to produce an Fe^{III}-superoxo intermediate, which would initiate a radical process involving two hydrogen atom abstractions from the bound amino group. The resulting substrate radical would undergo spontaneous conversion into products. The role of cosubstrate ascorbate is proposed to reduce the toxic peroxo byproduct to water.[23]

Obtaining information about the active sites in the non-heme Fe^{II} enzymes has been hampered relative to heme systems because the non-heme Fe^{II} center is less spectroscopically accessible, lacking strong absorption features and generally EPR silent. The application of NIR circular dichroism (CD), magnetic circular dichroism (MCD), and variable-temperature, variable-field (VTVH) MCD spectroscopies has greatly advanced the level of understanding of these systems as this methodology allows the direct observation of the Fe^{II} ligand-field (LF) transitions.[24,25] Fe^{II} has a ^5E_g LF excited state at 10 Dq (∼10000 cm^{-1}) above the $^5T_{2g}$ ground state. The energy of the d → d transitions gives the ^5E_g excited state, which is sensitive to the coordination number and geometry at the Fe^{II} center. Six-coordinate distorted octahedral Fe^{II} sites show two transitions at ∼10 000 cm^{-1}, split by ∼2 000 cm^{-1} ($\Delta^5E_g \approx 2000$ cm^{-1}), five-coordinate sites show one transition at ∼10 000 cm^{-1} and a second at ∼5 000 cm^{-1}, and distorted tetrahedral four-coordinate sites show transitions in the 4000−7000 cm^{-1} region.[25,26] VTVH MCD can further be used to obtain complementary ground-state electronic structure information. The MCD intensity for non-Kramers Fe^{II} centers shows an unusual temperature and field dependence, which is characterized by nested saturation magnetization behavior (i.e., nonsuperimposing isotherms when plotted vs $\beta H/2kT$). Ground-state information is obtained by numerically fitting experimental VTVH MCD data to an intensity expression (eq 1 in ref 27) that includes the spin Hamiltonian parameters of the ground state (δ and $g_{||}$ for a −ZFS system, and D and E for a +ZFS system), thus providing EPR-type information for EPR-inactive centers. The ground-state spin Hamiltonian parameters are directly related to the splitting of the $^5T_{2g}$ LF ground state ($\Delta \equiv d_{xz,yz} - d_{xy}$ and $V \equiv d_{xz} - d_{yz}$) for six- and five-coordinate sites. The combination of NIR CD, MCD, and VTVH MCD provides a complete description of the d-orbital energies for an Fe^{II} site, and has been applied to a number of non-heme iron enzymes to directly probe active site geometric and electronic structures and to gain mechanistic information about their catalytic cycles. On the basis of these studies, a general mechanistic strategy utilized by many of the non-heme Fe^{II} enzymes has been developed.[25,28]

We now apply this methodology to directly probe the geometric and electronic structure of the Fe^{II} active site in ACCO and its interaction with substrate ACC, cosubstrate ascorbate, and activator CO_2 to obtain insight into its catalytic mechanism and to define the role of CO_2 activation on a molecular level.

Experimental Section

Growth, Overexpression, and Purification of ACCO in *E. coli* BL21(DE3)pLysS. *E. coli* BL21(DE3)p*Lys*S/pETe3-4C2 possessing the AVOe3 gene was grown as previously described[23] or in M10 minimal media[29] with the following modifications. Cells were grown in 15 L carboys bubbled with air. M10 minimal media was supplemented with 1% casamino acids, 1% glucose, and 20 mL/L Hutner's mineral base,[30] which provides necessary trace metal cations. ACCO production was induced by the addition of β-D-thiogalactoside (IPTG) to a final concentration of 0.8 mM. IPTG was added while the cultures were still in the logarithmic phase (OD ≅ 0.5). Induction was carried out at 27 °C for 4 h. Cells were resuspended in 20 mM Bis-Tris at pH 6.0, 1.0 mM EDTA, 1.0 mM DTT, 10% glycerol, frozen in liquid nitrogen and stored at −80 °C. Purification was performed as previously described.[23]

Spectroscopy. All commercial reagents were used without further purification: MOPS buffer (Sigma), D_2O (99.9 atom % D; Aldrich), sodium deuterioxide (99+ atom % D; Sigma), sucrose (Sigma), ACC (Sigma), ascorbic acid sodium salt (Fluka), sodium bicarbonate (Aldrich), α-ketoglutaric acid (2-oxopentanedioic acid) sodium salt (Sigma), ferrous ammonium sulfate (FeAS, $[Fe(H_2O)_6](NH_4)_2(SO_4)_2$; MCB Manufacturing Chemists, Inc.). All samples for spectroscopy were prepared under an inert atmosphere inside a N_2-purged wet box. ApoACCO was made anaerobic by purging the apoenzyme with argon gas on a Schlenk line and alternating quick cycles of vacuum and argon. Fe^{II}, ACC, ascorbate, HCO_3^- (substituting CO_2 in all samples), and α-KG were added in microliter quantities from anaerobic stock solutions in degassed MOPS buffer, pD 7. Fresh stock solutions were prepared for each set of experiments.

(13) Zhang, Z. H.; Barlow, J. N.; Baldwin, J. E.; Schofield, C. J. *Biochemistry* **1997**, *36*, 15999−16007.
(14) Yang, S. F.; Hoffman, N. E. *Annu. Rev. Plant Physiol. Mol. Biol.* **1984**, *35*, 155−189.
(15) Dong, J. G.; Fernandez-Maculet, J. C.; Yang, S. F. *Proc. Natl. Acad. Sci. U.S.A.* **1992**, *89*, 9789−9793.
(16) Fernandez-Maculet, J. C.; Dong, J. G.; Yang, S. F. *Biochem. Biophys. Res. Commun.* **1993**, *193*, 1168−1173.
(17) Finlayson, S. A.; Reid, D. M. *Phytochemistry* **1994**, *35*, 847−851.
(18) Poneleit, L. S.; Dilley, D. R. *Postharvest Biol. Technol.* **1993**, *3*, 191−199.
(19) Vioque, B.; Castellano, J. M. *J. Agric. Food Chem.* **1998**, *46*, 1706−1711.
(20) Barlow, J. N.; Zhang, Z. H.; John, P.; Baldwin, J. E.; Schofield, C. J. *Biochemistry* **1997**, *36*, 3563−3569.
(21) Charng, Y.-y.; Liu, Y.; Dong, J. G.; Yang, S. F. In *Biology and biotechnology of the plant hormone ethylene*; Kanellis, A. K., Chang, C., Kende, H., Grierson, D., Eds.; Kluwer Academic Publishers: Dordrecht/Boston/London, 1997; pp 23−29.
(22) Pirrung, M. C.; Cao, J.; Chen, J. *Chem. Biol.* **1998**, *5*, 49−57.
(23) Rocklin, A. M.; Tierney, D. L.; Kofman, V.; Brunhuber, N. M. W.; Hoffman, B. M.; Christoffersen, R. E.; Reich, N. O.; Lipscomb, J. D.; Que, L. *Proc. Natl. Acad. Sci. U.S.A.* **1999**, *96*, 7905−7909.
(24) Solomon, E. I.; Pavel, E. G.; Loeb, K. E.; Campochiaro, C. *Coord. Chem. Rev.* **1995**, *144*, 369−460.
(25) Solomon, E. I.; Brunold, T. C.; Davis, M. I.; Kemsley, J. N.; Lee, S. K.; Lehnert, N.; Neese, F.; Skulan, A. J.; Yang, Y. S.; Zhou, J. *Chem. Rev.* **2000**, *100*, 235−349.
(26) Solomon, E. I.; Penfield, K. W.; Gewirth, A. A.; Lowery, M. D.; Shadle, S. E.; Guckert, J. A.; LaCroix, L. B. *Inorg. Chim. Acta* **1996**, *243*, 67−78.
(27) Pavel, E. G.; Kitajima, N.; Solomon, E. I. *J. Am. Chem. Soc.* **1998**, *120*, 3949−3962.
(28) Zhou, J.; Gunsior, M.; Bachmann, B. O.; Townsend, C. A.; Solomon, E. I. *J. Am. Chem. Soc.* **1998**, *120*, 13539−13540.
(29) Okar, D. A.; Felicia, N. D.; Gui, L.; Lange, A. J. *Protein Expression Purif.* **1997**, *11*, 79−85.
(30) Cohen-Bazire, G.; Sistrom, W. R.; Stanler, R. Y. *J. Cell. Comput. Physiol.* **1957**, 25−68.

Samples for CD spectroscopy (3−4 mM apoACCO) were kept anaerobic in a custom-made 1 cm path length masked optical cell (Wilmad) fitted with a gastight Teflon stopcock (LabGlass). Titration additions into the anaerobic optical cell were carried out in the wet box using gastight syringes fitted with custom 5 in. long needles (Hamilton Co.). Addition of 60% (v/v) glycerol-d_3 alters the CD spectra of ACCO; thus, glycerol could not be used as a glassing agent for low-temperature MCD spectroscopic studies on these complexes. Addition of saturated sucrose does not alter the CD spectra; thus, the low-temperature MCD spectroscopic studies on these ACCO complexes used saturated sucrose as a glassing agent. Samples for MCD spectroscopy (1.5−2 mM apoACCO) were prepared by the anaerobic addition of FeAS to the apoenzyme, followed by addition of saturated sucrose. MCD samples were injected into a cell with a 0.3-cm thick neoprene spacer sandwiched between two infrasil quartz disks and secured between two copper plates; cells were frozen under liquid N_2 immediately upon removal from the wet box.

Instrumentation. NIR (600−2000 nm) CD and MCD spectra were recorded on a Jasco J200D spectropolarimeter with a liquid N_2-cooled InSb detector and an Oxford Instruments SM4000-7T superconducting magnet/cryostat (0−7 T, 1.5−300 K). UV/vis (300−850 nm) CD spectra were obtained on a Jasco J810 spectropolarimeter with an extended S-20 photomultiplier tube (Hammamatsu). CD samples were maintained at a temperature of 278 K using a recirculating water bath and thermostatic cell holder (HP) on each spectropolarimeter. CD spectra are baseline corrected by subtracting the buffer and cell backgrounds from the raw data. Depolarization of frozen MCD samples was judged to be <5% from comparison of the CD spectra of a nickel (+)-tartrate solution placed before and after the sample. The reported MCD spectra and the VTVH MCD data are the averaged subtraction of the negative field raw data from the positive field raw data, which avoids subtraction problems due to baseline shifts in poor-quality frozen glasses.

Fitting Procedures. Saturation magnetization data were normalized to the maximum observed intensity and fit according to published procedures to extract ground-state parameters. Both the negative and the positive ZFS models were applied to the VTVH MCD data to determine the best fit. Binding constants were estimated from CD titration data using the method of Rose and Drago.[31]

Results and Analysis

A. NIR CD Titrations of ACC, Ascorbate, CO_2, and α-KG Binding to ACCO. NIR CD spectroscopy has been used to probe substrate ACC and the cosubstrate ascorbate binding to ACCO/Fe^{II} both in the presence and absence of CO_2 (supplied as HCO_3^-) and to estimate binding constants.

1. ACCO/Fe^{II} and Its Interaction with HCO_3^- and Ascorbate. Apo-ACCO shows no CD signal in the NIR region (from 5000 to 16000 cm^{-1}). Addition of Fe^{II} in the absence of CO_2 results in a weak, broad, positive band at ~9000 cm^{-1} ($\Delta\epsilon \sim +0.025$ cm^{-1} M^{-1}) that can be resolved into two Gaussian peaks at 8950 and 10550 cm^{-1}, corresponding to the LF transitions for an Fe^{II} site (Figure 1c, blue line). Because neither the apoenzyme nor the aqueous FeAS contribute to the CD spectrum, these d → d bands must be due to a six-coordinate Fe^{II} bound to the ACCO enzyme at the active site. Addition of HCO_3^-, up to 50 equiv relative to ACCO, results in no change in the CD spectrum (Figure 1a, blue line), indicating that CO_2 has no significant effect on the resting ACCO/Fe^{II} site. Addition of up to 30 equiv of ascorbate causes a small intensity change to the weak NIR CD signal of the ACCO/Fe^{II} complex in the absence but not in the presence of CO_2 (data not shown).

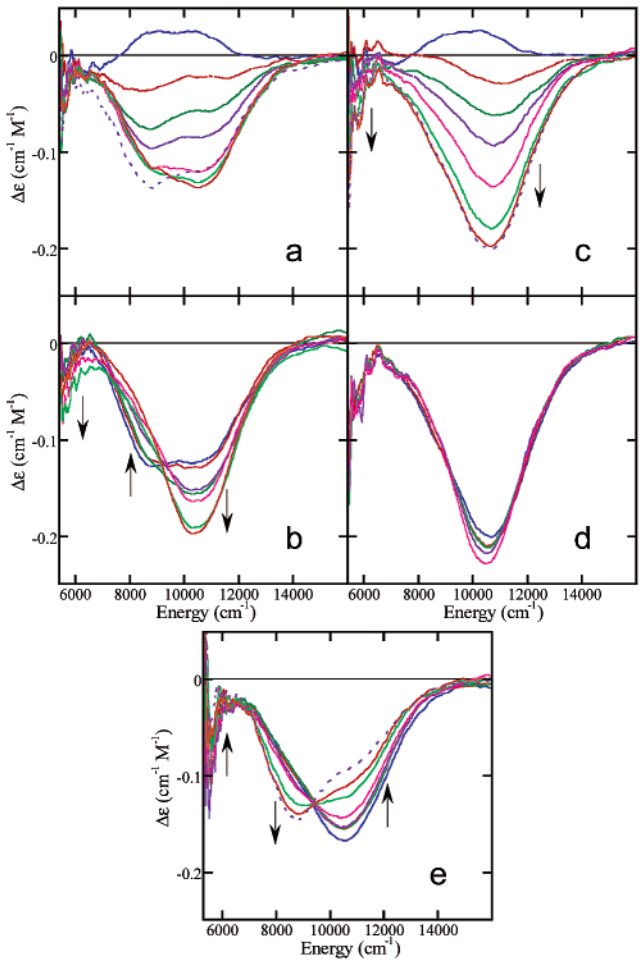

Figure 1. NIR CD titration studies (at 4 °C) of substrate ACC and cosubstrate ascorbate binding to ACCO/Fe^{II} in the presence (a and b) and absence of CO_2 (c and d) and CO_2 binding to ACCO/Fe^{II}/ACC (e). (a) ACCO (3.8 mM)/Fe^{II} (0.8 equiv, all equivalents relative to apoACCO) complex in the presence of CO_2 (30 equiv) with addition of 0 (blue line), 0.5, 1, 2, 5, 10, and 20 (orange line) equiv of ACC and further addition of 20 equiv of CO_2 (purple dashed line); (b) ACCO (3.0 mM)/Fe^{II} (0.8 equiv)/ACC (30 equiv) complex in the presence of CO_2 (30 equiv) with addition of 0 (blue line), 0.5, 1, 2, 5, 10, and 20 (orange line) equiv of ascorbate; (c) ACCO (3.8 mM)/Fe^{II} (0.8 equiv) complex in the absence of CO_2 with addition of 0 (blue line), 0.5, 1, 2, 5, 10, 20, and 30 (purple dashed line) equiv of ACC; (d) ACCO (3.5 mM)/Fe^{II} (0.8 equiv)/ACC (30 equiv) complex in the absence of CO_2 with addition of 0 (blue line), 0.5, 1, 2, 5, and 10 (pink line) equiv of ascorbate; (e) ACCO (3.5 mM)/Fe^{II} (0.8 equiv)/ACC (30 equiv) complex with addition of 0 (blue line), 0.5, 1, 2, 5, 10, 20, and 50 (purple dashed line) equiv of CO_2.

2. ACC and Ascorbate Binding in the Presence of CO_2. In contrast to the negligible effect on the ACCO/Fe^{II} site by the binding of CO_2 and/or ascorbate, the binding of the substrate ACC causes a dramatic change in the intensity and the sign of the NIR CD signal of the ACCO/Fe^{II} complex in the presence (and absence, vide infra) of CO_2. Figure 1a shows the NIR CD titration of ACC binding to ACCO/Fe^{II} in the presence of CO_2 (increasing equivalents of ACC were added to ACCO + 0.8 equiv of Fe^{II} + 30 equiv of HCO_3^-). Upon addition of 0.5 equiv of ACC, the weak positive band of ACCO/Fe^{II}/CO_2 (Figure 1a, blue line) disappears and a negative band appears (Figure 1a, red line). The titration was complicated by the loss of CO_2 during the experiment, indicated by band shape changes at later stages of titration which could be reversed by the further addition of 20 equiv of HCO_3^- (Figure 1a, purple dashed line, $\Delta\epsilon \sim -0.14$ cm^{-1} M^{-1} at 8900 cm^{-1}). A dissociation constant for

(31) Connors, K. A. *Binding Constants: The Measurement of Molecular Complex Stability*; John Wiley & Sons: New York; Chapter 4, 1987.

ACC binding to the ACCO/Fe^{II}/CO_2 complex was estimated to be $K_d = 0.5 \pm 0.3$ mM by fitting the intensity at 9360 cm^{-1}, which is an isosbestic point in HCO_3^- titration (see Figure 1e). The lower limit of this K_d (0.2 mM) is somewhat higher than the K_m of 0.06 mM from steady-state kinetic studies.[32]

An additional NIR CD titration probed ascorbate binding to the ACCO/Fe^{II}/CO_2/ACC complex (Figure 1b). Addition of increasing amounts ascorbate to ACCO + 0.8 equiv of Fe^{II} + 30 equiv of HCO_3^- + 20 equiv of ACC caused significant changes in the CD spectrum. A negative low-energy reproducible band at ~5 000 cm^{-1} developed with a concomitant intensity decrease at ~8 800 cm^{-1} and intensity increase at ~10 400 cm^{-1}. The changes saturate between 10 and 20 equiv and a dissociation constant for ascorbate binding to the ACCO/Fe^{II}/CO_2/ACC complex was estimated as $K_d = 4 \pm 3$ mM, consistent with the steady-state kinetic result ($K_m = 2.1$ mM).[32] The final ACCO/Fe^{II}/CO_2/ACC/ASC complex had two bands in the NIR CD spectrum, one at ~5 000 cm^{-1} and the other at 10 400 cm^{-1}, indicating a major five-coordinate Fe^{II} site is present in this complex.

3. ACC and Ascorbate Binding in the Absence of CO_2. Parallel NIR CD titrations of ACC and ascorbate binding to ACCO/Fe^{II} in the absence of CO_2 were also carried out to probe the effect of CO_2 and are presented in Figure 1, parts c and d, respectively. As increasing amounts of ACC were added to ACCO + 0.8 equiv of Fe^{II}, a low-energy negative reproducible band at ~5 000 cm^{-1} and a higher energy negative band at 10 600 cm^{-1} developed simultaneously. These changes saturate between 20 and 30 equiv of ACC and a dissociation constant for ACC binding to ACCO/Fe^{II} in the absence of CO_2 was estimated at 3.5 ± 1.5 mM, indicating weaker binding of ACC to ACCO/Fe^{II} than in the presence of CO_2. The CD spectrum of the resultant ACCO/Fe^{II}/ACC species is very different from that of the ACCO/Fe^{II}/CO_2/ACC complex (Figure 1a, purple dashed line) but resembles that of the ACCO/Fe^{II}/CO_2/ACC/ascorbate complex (Figure 1b, orange line) and is consistent with a five-coordinate Fe^{II} site in the ACCO/Fe^{II}/ACC complex in the absence of CO_2. Further addition of ascorbate to the above ACCO/Fe^{II}/ACC complex (Figure 1d) results in some additional intensity increase at 10 600 cm^{-1}.

4. CO_2 Binding to ACCO/Fe^{II}/ACC. The effects of CO_2 binding to the ACCO/Fe^{II}/ACC complex were further studied by a CD titration of HCO_3^- into ACCO + 0.8 equiv of Fe^{II} + 20 equiv of ACC (Figure 1e). The NIR CD spectrum of ACCO/Fe^{II}/ACC has two negative bands at ~5 000 and 10 400 cm^{-1}. Addition of HCO_3^- changed the band shape of the high-energy band (shifting the peak maximum from 10 400 to 8 800 cm^{-1}) and significantly decreased the intensity of the low-energy band at ~5000 cm^{-1}. The isosbestic point at 9360 cm^{-1} indicates that there are only two species in the titration and a dissociation constant for HCO_3^- binding to ACCO/Fe^{II} was estimated as $K_d = 1.5 \pm 1$ mM (corresponding to 0.3 ± 0.06 mM for aqueous CO_2, comparing well with $K_m = 0.2$ mM for apple ACCO). This clearly confirms that the ACCO/Fe^{II}/ACC complex, mainly a five-coordinate species, becomes six-coordinate on addition of CO_2.

5. Inhibitor α-KG Binding. NIR CD titrations were also used to study the binding of the α-KG inhibitor to ACCO/Fe^{II}

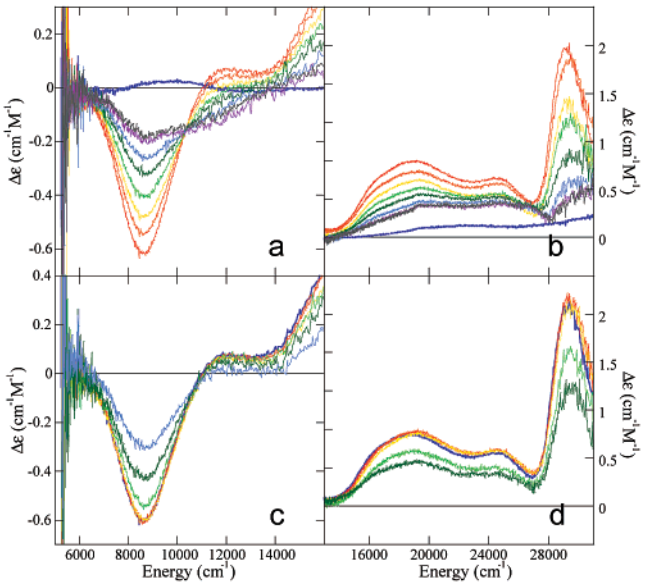

Figure 2. NIR and UV/vis CD titration studies (at 4 °C) of the α-KG inhibitor binding to ACCO/Fe^{II} in the absence of CO_2. NIR CD spectra (a) and UV/vis CD spectra (b) of the ACCO (3.5 mM)/Fe^{II} (0.8 equiv)/α-KG (20 equiv) complex with addition of 0 (red line), 5, 10, 20, 50, 100, 200, and 350 (gray line) equiv of ACC; NIR CD spectra (c) and UV/vis CD spectra (d) of the ACCO/Fe^{II}/α-KG (20 equiv) complex with addition of 0 (red line), 5, 10, 50, 100, 350, and 850 (gray line) equiv of ascorbate.

in the absence of CO_2, and its competition with ACC and ascorbate. The dark blue lines in Figure 2a,b are the CD spectra of ACCO/Fe^{II}, which show a weak band in the NIR region (~10 000 cm^{-1}, Figure 2a) and a featureless small slope in the UV/vis region (Figure 2b). Addition of 20 equiv of α-KG produced a pink color in the sample. The NIR CD spectrum shows a strong asymmetric negative band ($\Delta\epsilon = -0.6$ cm^{-1} M^{-1} at 8600 cm^{-1}) with no intensity in the low-energy region (~5000 cm^{-1}), which indicates that a six-coordinate ACCO/Fe^{II}/α-KG complex is formed. There is a broad positive band in the visible region ($\Delta\epsilon = 0.77$ cm^{-1} M^{-1} at 19 000 cm^{-1}, and $\Delta\epsilon = 0.61$ cm^{-1} M^{-1} at 24 500 cm^{-1}), and a sharp positive band in the near-UV region ($\Delta\epsilon = 2.0$ cm^{-1} M^{-1} at 29 200 cm^{-1}). These spectral features are very similar to those of the Fe^{II}/α-KG complex of the α-KG-dependent enzyme CS2. The transitions of CS2/Fe^{II}/α-KG complex have been assigned as the Fe^{II}-to-α-KG charge transfer (CT) and α-KG n → π^* transitions and are characteristic of the bidentate binding mode of α-KG directly to Fe^{II} through the 1-carboxylate and 2-carbonyl groups in CS2.[33] Thus, in the ACCO/Fe^{II}/α-KG complex, α-KG adopts a similar bidentate binding mode. Figure 2a,b also shows the titration of ACC to the ACCO + 0.8 equiv of Fe^{II} + 20 equiv of α-KG, as monitored in the NIR and UV/vis region, respectively, and Figure 2c,d shows the parallel ascorbate titration studies. Addition of substrate ACC or ascorbate results in an intensity decrease for all the α-KG CT transitions (Figure 2, parts b and d, respectively) and spectral changes for the Fe^{II} d → d transitions (Figure 2, parts a and c, respectively) of the ACCO/Fe^{II}/α-KG complex. For ACC, the intensities are halved when 20 equiv of ACC was added (Figure 2a,b, light green line) while 350 equiv of ascorbate was needed to halve the α-KG intensity. This indicates a significantly lower enzyme affinity for ascorbate than for ACC in the absence of CO_2. An α-KG

(32) Brunhuber, N. M. W.; Mort, J. L.; Christoffersen, R. E.; Reich, N. O. *Biochemistry* **2000**, *39*, 10730−10738.

(33) Pavel, E. G.; Zhou, J.; Busby, R. W.; Gunsior, M.; Townsend, C. A.; Solomon, E. I. *J. Am. Chem. Soc.* **1998**, *120*, 743−753.

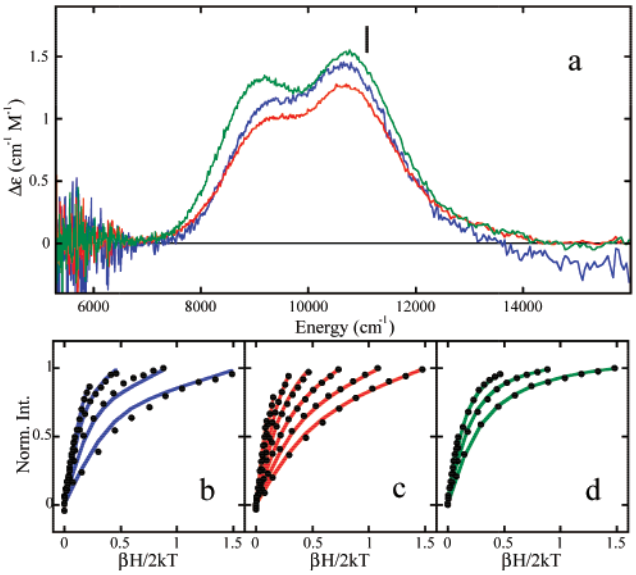

Figure 3. NIR VTVH MCD studies of the resting ACCO (1.5 mM)/Fe^{II} (0.8 equiv) complex and the effect of CO_2 (30 equiv) and ascorbate (30 equiv). NIR MCD spectra (5 K, 7 T) of the ACCO /Fe^{II} (a, blue line), ACCO/Fe^{II}/CO_2 (a, red line), and ACCO/Fe^{II}/ascorbate (a, green line) complexes; VTVH MCD data (•) plotted vs $\beta H/2kT$ with best fit (lines) of the ACCO/Fe^{II} (b), ACCO/Fe^{II}/CO_2 (c), and ACCO/Fe^{II}/ascorbate (d) complexes. The best fits to the data were generated with the parameters summarized in Table 1.

dissociation constant was estimated at ~3.5 mM from the ACC dissociation constant in the absence of CO_2. This is somewhat higher than the steady-state kinetic result (K_i = 1.35 mM). These results demonstrate that both ACC and ascorbate displace α-KG from the Fe^{II} site.

B. NIR VTVH MCD Studies of the ACCO/Fe^{II}, ACCO/Fe^{II}/Ascorbate, ACCO/Fe^{II}/ACC, and ACCO/Fe^{II}/ACC/Ascorbate Complexes, in the Presence and Absence of CO_2. 1. Resting ACCO/Fe^{II} and the Effect of CO_2 and Ascorbate. Figure 3a shows the 5 K 7 T MCD spectra of the resting ACCO/Fe^{II} complex (blue line), the ACCO/Fe^{II}/CO_2 complex (red line), and the ACCO/Fe^{II}/ascorbate complex (green line). The blue and red spectra are very similar and both can be resolved into two Gaussian bands at 9 200 and 11 100 cm^{-1} to give Δ^5E_g of 1 800 cm^{-1} (see Table 1). These are consistent with the CD studies of the ACCO/Fe^{II} complex and the ACCO/Fe^{II}/CO_2 complex, indicating that a similar distorted six-coordinate Fe^{II} site is present in both complexes. The 5 K, 7 T MCD spectrum of ACCO/Fe^{II}/ascorbate (green line in Figure 3a) shows a small shift of the low-energy band to lower energy and thus a small increase in Δ^5E_g to 2000 cm^{-1} (see Table 1). The 5 K, 7 T MCD spectrum of the ACCO/Fe^{II}/CO_2/ascorbate complex is very similar to that of ACCO/Fe^{II}/CO_2 (data not shown).

VTVH MCD was used to probe the ground-state splittings of the above three complexes by monitoring the MCD intensities at both 9 000 and 11 100 cm^{-1}, which result in the same behavior. The VTVH MCD data at 11 100 cm^{-1} of ACCO/Fe^{II}, ACCO/Fe^{II}/CO_2, and ACCO/Fe^{II}/ascorbate are shown in Figure 3,parts b, c, and d, respectively, with their best fit. All three sets of VTVH data are fit by a +ZFS non-Kramers model, and the ground-state spin Hamiltonian parameters obtained are listed in Table 1. The results for ACCO/Fe^{II} and ACCO/Fe^{II}/CO_2 are virtually the same, while those of ACCO/Fe^{II}/ASC show a smaller +D value (consistent with a smaller nesting)

Table 1. Ligand Field MCD Transition Energies, Ground-State Spin Hamiltonian Parameters, and Ligand Field Parameters

	ACCO/Fe^{II}/				ACCO/Fe^{II}/ASC		ACCO/Fe^{II}/ACC		ACCO/Fe^{II}/ACC/ASC	
±CO_2	+CO_2	−CO_2	+CO_2	−CO_2	+CO_2	−CO_2	+CO_2	−CO_2	+CO_2	−CO_2
peak positions[c]	9200, 11000	9200, 11000	9200, 11000	9000, 11000	9200, 11250	~5000, 9300, 11100	~5000, 9300, 11400	~5000, 9300, 11000		
energy splitting[c]	1800	1800	1800	2000	2050	~4300, 1800	~4300, 2100	~4300, 1800		
VTVH positions[c]	11100	11100	11100	11100	8850 11100	7520 11100	8330 11100	7870 11100		
$-D$										
δ[c]					3.5 ± 0.2	3 ± 0.1	3.5 ± 0.1	3.5 ± 0.1		
$g_{\|\|}$					9.2 ± 0.2	9 ± 0.1	9.1 ± 0.1	9.1 ± 0.1		
M_z/M_{xy}[a]					−0.2 −0.1	−0.2	−0.1	−0.5		
B-term[b]					0.3 2.5	0.1	0.5	−1		
$+D$										
D[c]	11 ± 1	9 ± 1	9 ± 1	8 ± 1					10 ± 1	10 ± 1
$\|E\|$[c]	1 ± 0.2	1 ± 0.1	1 ± 0.1	1.6 ± 0.1					2 ± 0.2	2 ± 0.2
M_z/M_{xy}[a]	0.25	0.8	0.05	0.2					0.3	−0.3
B-term[b]	2.9	3.5	0.04	0.9					4.4	4.2
Δ[c]	600 ± 100	800 ± 150	800 ± 200	1000 ± 250	−500 ± 200	−800 ± 100	−500 ± 200	−700 ± 100	750 ± 150	−700 ± 100	750 ± 150
$\|V/2\Delta\|$	0.12 ± 0.01	0.06 ± 0.02	0.15 ± 0.04	0.25 ± 0.05	0.23 ± 0.07	0.26 ± 0.04	0.23 ± 0.07	0.26 ± 0.02	0.27 ± 0.05	0.26 ± 0.02	0.27 ± 0.05
$\|V\|$[c]	150 ± 50	100 ± 50	250 ± 100	500 ± 250	250 ± 150	400 ± 100	250 ± 150	400 ± 100	420 ± 150	400 ± 100	420 ± 150

[a] For $g_\perp$ fixed at 1.0. [b] Reported as a percentage of the C-term intensity scaling factor (see ref 24). [c] Units: cm^{-1}.

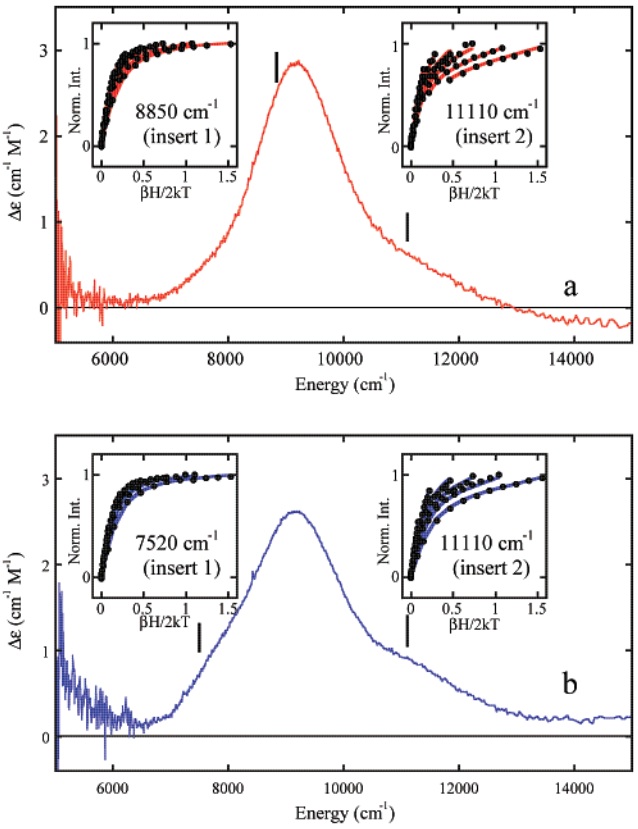

Figure 4. NIR MCD studies of theACCO (1.4 mM) /Fe^{II} (0.8 equiv)/ACC (30 equiv) complex and the effect of CO_2. (a) NIR MCD spectra (5 K, 7 T) of the ACCO/Fe^{II}/CO_2/ACC complex and its VTVH MCD data (•) at 8850 cm^{-1} (insert 1) and at 11100 cm^{-1} (insert 2) plotted vs $\beta H/2kT$ with best fit (lines); (b) NIR MCD spectra (5 K, 7 T) of the ACCO/Fe^{II}/ACC complex and its VTVH MCD data at 7520 cm^{-1} (insert 1) and at 11100 cm^{-1} (insert 2). The best fits to the data were generated with the parameters summarized in Table 1.

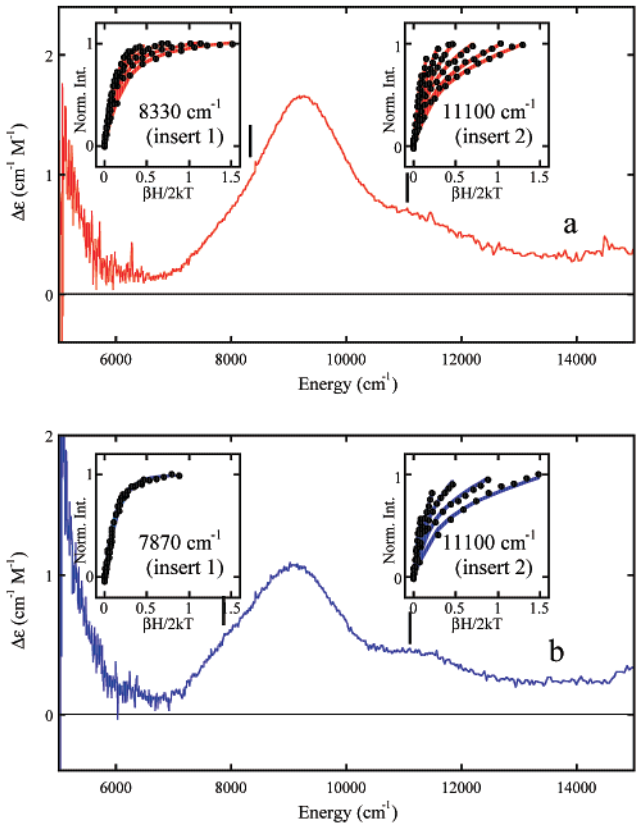

Figure 5. NIR MCD studies of theACCO (1.4 mM)/Fe^{II} (0.8 equiv)/ACC (30 equiv)/ascorbate (30 equiv) complex and the effect of CO_2. (a) NIR MCD spectra (5 K, 7 T) of the ACCO/Fe^{II}/CO_2/ACC/ascorbate complex and its VTVH MCD data (•) at 8330 cm^{-1} (insert 1) and at 11100 cm^{-1} (insert 2) plotted vs $\beta H/2kT$ with best fit (lines); (b) NIR MCD spectra (5 K, 7 T) of the ACCO/Fe^{II}/ACC/ascorbate complex and its VTVH MCD data at 7870 cm^{-1} (insert 1) and at 11100 cm^{-1} (insert 2). The best fits to the data were generated with the parameters summarized in Table 1.

and thus a larger $^5T_{2g}$ splitting. The values obtained are all within the range expected for a distorted six-coordinate site. Thus from the CD, MCD, and VTVH MCD data, the resting ACCO/Fe^{II} contains a high-spin Fe^{II} active site with a six-coordinate distorted octahedral geometry and CO_2 binding has little effect on ACCO/Fe^{II} while ascorbate binding results in a slightly different six-coordinate site, consistent with the CD results.

2. ACCO/Fe^{II}/ACC Complex and the Effect of CO_2. Figure 4 shows the NIR MCD spectra at 5 K, 7 T of the ACCO/Fe^{II}/ACC complex in the presence (Figure 4a) and absence of CO_2 (Figure 4b). The NIR MCD spectrum of the ACCO/Fe^{II}/ACC complex in the presence of CO_2 contains one intense band at 9200 cm^{-1} with a smaller shoulder at ~11 250 cm^{-1} (Figure 4a), indicating only one species is present. There is no measurable signal above the noise in the low-energy region (~5000 cm^{-1}). The VTVH MCD data taken at the two energies look different (Figure 4a, inserts 1 and 2) but can be fit with the same set of ground-state parameters using the −ZFS non-Kramers model with a larger *B*-term (due to a polarization difference) for the data at ~11 100 cm^{-1} (see Table 1). This is consistent with the presence of only one species in the ACCO/Fe^{II}/CO_2/ACC complex. The much larger MCD intensity and the different ground-state parameters obtained from the VTVH data relative to the ACCO/Fe^{II}/CO_2 complex are consistent with a new six-coordinate Fe^{II} site in the ACCO/Fe^{II}/ACC complex in the presence of CO_2.

The NIR MCD spectrum of the ACCO/Fe^{II}/ACC complex in the absence of CO_2 has four bands (Figure 4b), requiring the presence of more than one species. Comparison to the NIR MCD spectrum of the ACCO/Fe^{II}/ACC complex in the presence of CO_2 (Figure 4a) indicates that a new low-energy temperature-dependent band is present at ~5000 cm^{-1} (see Figure 1Sa in the Supporting Information for the temperature dependence of this band) and that the shoulders at ~8 000 cm^{-1} and ~11 100 cm^{-1} are more pronounced. The presence of a ~5 000 cm^{-1} transition combined with an additional transition in the ~10 000 cm^{-1} region indicates that a five-coordinate Fe^{II} site is present in the ACCO/Fe^{II}/ACC complex in the absence of CO_2. The low-energy band is too weak to obtain reliable VTVH MCD data. VTVH MCD data were taken on the low- and high-energy sides of the higher energy bands (at 7 520 and 11 100 cm^{-1}, Figure 4b, inserts 1 and 2, respectively). The data at 7520 cm^{-1} can be fitted with a −ZFS model and the ground-state parameters obtained (Table 1) are consistent with a five-coordinate species contributing intensity at the ~8000 cm^{-1} shoulder. The energy position of the band and the VTVH data at 11 100 cm^{-1} (Figure 4**b** insert 2) with best fits (Table 1) are consistent with the assignment of a six-coordinate species also present in the ACCO/Fe^{II}/ACC in the absence of CO_2.

3. ACCO/Fe^{II}/ACC/ASC Complex and the Effect of CO_2. Figure 5 shows the NIR MCD spectra at 5 K, 7 T of the ACCO/Fe^{II}/ACC/ASC complex in the presence (Figure 5a) and absence

Scheme 1

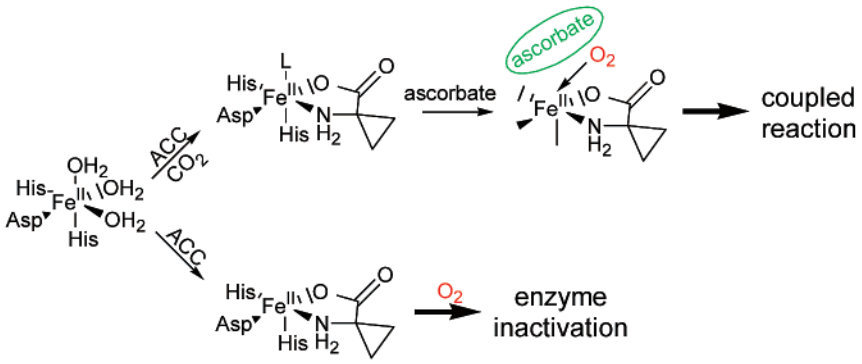

of CO_2 (Figure 5b). In contrast to the NIR MCD spectrum of the ACCO/Fe^{II}/ACC complex in the presence of CO_2, ascorbate binding results in the presence of a stronger temperature-dependent low-energy band at ~5000 cm^{-1} (see Figure 1Sb in the Supporting Information for the temperature dependence of this band), consistent with CD studies, which indicates that a five-coordinate species is formed upon ascorbate binding. The low-energy band is too noisy to obtain reliable VTVH data. The VTVH MCD data taken at 8 330 and 11 100 cm^{-1} (Figure 5a ,inserts 1 and 2, respectively) have very different nesting behaviors and can be fit with two different sets of ground-state parameters (see Table 1). This is consistent with the fact that more than one species contributes to the MCD intensity around 10 000 cm^{-1}. The ground-state parameters obtained from the VTVH data at 11 100 cm^{-1} indicate the presence of a six-coordinate Fe^{II} site in the ACCO/Fe^{II}/ACC/ascorbate complex in the presence of CO_2, in addition to the five-coordinate Fe^{II} species.

The NIR MCD spectrum of the ACCO/Fe^{II}/ACC/ascorbate complex in the absence of CO_2 (Figure 5b) shows a stronger low-energy band at ~5000 cm^{-1} (see Figure 1Sc in the Supporting Information for the temperature dependence of this band) than that present in the ACCO/Fe^{II}/ACC complex (Figure 4b). The former is more similar to that of the ACCO/Fe^{II}/ACC/ascorbate complex in the presence of CO_2 (Figure 5a). The presence of a ~5 000 cm^{-1} transition combined with transitions in the ~10 000 cm^{-1} region indicate that a five-coordinate Fe^{II} site is present in the ACCO/Fe^{II}/ACC/ASC complex in the absence of CO_2. Again, the pronounce shoulder on the high-energy band shows that more than one species is present. VTVH MCD data were taken on the low- and high-energy sides of the higher energy band (at 7870 and 11100 cm^{-1}, Figure 5b, inserts 1 and 2, respectively). The data at 7870 cm^{-1} can be fit with a −ZFS model while the data at 11 100 cm^{-1} require a +ZFS model (see Table 1). The energy position and the VTVH data at 11 100 cm^{-1} (Figure 5b, insert 2) with best fits (Table 1) are consistent with the assignment of a six-coordinate species also present in the ACCO/Fe^{II}/ACC/ascorbate complex in the absence of CO_2.

The relative amount of the five-coordinate species present in the ACCO/Fe^{II}/ACC, ACCO/Fe^{II}/ACC/CO_2/ascorbate, and ACCO/Fe^{II}/ACC/ascorbate complexes can be estimated by comparing the intensities of the NIR MCD bands at ~5000 (five-coordinate), 9200 (mainly six-coordinate, overlapping with five-coordinate), and 11 000 cm^{-1} (six-coordinate). Approximately 70% conversion from a six-coordinate species to a five-coordinate species was estimated for the ACCO/Fe^{II}/ACC/ascorbate complex relative to the ACCO/Fe^{II}/ACC/CO_2 complex. Approximately 50% of the Fe^{II} species in the ACCO/Fe^{II}/ACC/CO_2/ascorbate complex is five-coordinate while 30% is five-coordinate in the ACCO/Fe^{II}/ACC complex. The amount of the five-coordinate species observed in MCD (5 K) appears to be less than that in CD (5 °C). This may be a temperature effect, with low temperature (MCD) stabilizing the six-coordinate component.

Discussion

The NIR CD, MCD, and VTVH MCD studies give electronic and geometric structural information about the Fe^{II} active site in ACCO and its interactions with the substrate ACC and the cosubstrate ascorbate, both in the presence and absence of CO_2, and with the inhibitor α-KG. In the presence of CO_2, resting ACCO/Fe^{II} has a six-coordinate distorted octahedral Fe^{II} site. This site shows only a small perturbation upon ascorbate binding, but changes into a significantly different six-coordinate site upon substrate ACC binding. This is clear from Figure 1a and Figure 4a vs. Figure 3a. Upon binding both ACC and ascorbate, the site goes mostly five-coordinate (see Figures 1b and 5a). In the absence of CO_2, resting ACCO/Fe^{II} is also six-coordinate and remains six-coordinate upon ascorbate binding as shown in Figure 3. However, upon substrate ACC binding in the absence of CO_2, ~30% of the Fe^{II} sites become five-coordinate (see Figures 1c and 4b). When both ACC and ascorbate are bound, the site is further converted to a major five-coordinate component similar to that observed with both ACC and ascorbate bound in the presence of CO_2 (Figures 1d,b and 5a,b).

The above results are consistent with the model shown in the top part of Scheme 1 for the first two steps in the mechanism for ACCO catalysis in the presence of CO_2. Fe^{II} binds to the active site to form a six-coordinate distorted octahedral site. ACC binds to the Fe^{II} center most likely in a bidentate mode through its 1-amino and 1-carboxylate group, as determined from the ENDOR and EPR studies[23] on the ACCO/Fe^{II}/NO complex, leading to a new six-coordinate species. The cosubstrate ascorbate then binds to the enzyme, thereby inducing a conformational change that results in the dissociation of an Fe^{II} ligand to form a five-coordinate site. The open coordination position on Fe^{II} could allow rapid O_2 binding and activation to generate an oxygen intermediate to initiate electron transfer from ACC. Thus, in the presence of CO_2, ACCO utilizes a similar mechanistic strategy for O_2 activation as observed in other cosubstrate-dependent mononuclear non-heme enzymes (six- to

Scheme 2

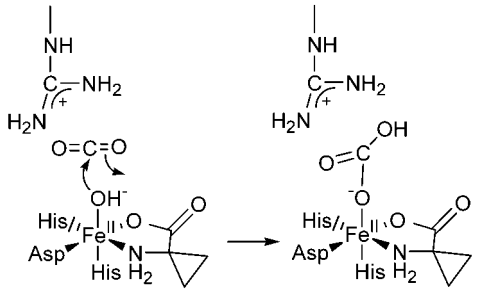

five-coordinate conversion only in the presence of (co)-substrates).[25,28,34]

Also from the CD and MCD studies, in the absence of CO_2, the binding of the substrate ACC produces ~30% five-coordinate Fe^{II} site while α-KG binding results in a pure six-coordinate species, despite the fact that both bind to Fe^{II} in a bidentate mode. As demonstrated by the smaller value of 10 Dq (9550 cm^{-1}) of the ACCO/Fe^{II}/α-KG complex than the 10 Dq (10250 cm^{-1}) of the ACCO/Fe^{II}/ACC complex in the presence of CO_2, the amino group of ACC is a stronger σ-donor than the carbonyl group of α-KG. Direct binding by the substrate amino group would result in less positive charge on the Fe^{II} ion thus destabilizing a water ligand and favoring a five-coordinate species. This is similar to the effect of substrate ACV binding in IPNS, where the direct binding of its thiolate group of the substrate ACV, which is a strong σ-donor ligand, also results in a five-coordinate substrate complex.[9] This will lead to dioxygen activation in both the ACCO/Fe^{II}/ACC and IPNS/Fe^{II}/ACV complexes. However, unlike ACV, which can supply four electrons from two oxidative ring-closures, ACC can only supply two electrons to activated dioxygen. Thus reaction in the absence of another electron donor would result in the oxidation of the active site and inactivation of the enzyme (Scheme 1, bottom). Thus in the case of ACCO, CO_2 is necessary to stabilize the six-coordinate ACCO/Fe^{II}/ACC complex, unless the cosubstrate is also bound to the enzyme to supply the other two electrons. Studies on ACCO under various conditions demonstrate that CO_2 plays a major role in decreasing the rate of deactivation.[20] Therefore, the role of CO_2 in the ACCO mechanism appears to prevent uncoupled oxidation when only ACC is bound.[35] One possible model for this is through bicarbonate formation. The coordinated water in the ACCO/Fe^{II} complex should have a pK_a ~ 9.5,[36] which would be low enough to catalyze the formation of a bicarbonate ligand by facilitating the nucleophilic attack of a hydroxide group onto the carbon atom of CO_2 at neutral pH (Scheme 2). The bicarbonate would be a stronger electron donor than the water and could be further stabilized by an electrostatic interaction with a C-terminal arginine group, which is conserved for all known ACCO enzymes. Alternatively, the CO_2 could bind to Fe^{II} as a linear nonhydrated species suggested by a recent crystal structure of DAOCS/Fe^{II}/succinate/CO_2 complex.[37]

In summary, this study has resulted in the following mechanistic insights for ACCO: (1) The resting ACCO/Fe^{II} complex has a six-coordinate distorted octahedral site. (2) In the presence of CO_2, ACC binding converts the iron site into a different six-coordinate distorted octahedral site. (3) Upon binding ascorbate, the site is converted to a major five-coordinate approximately square pyramidal site. This is consistent with the general mechanistic strategy for O_2 activation now determined to occur in a number of the mononuclear non-heme iron enzymes. (4) In the absence of CO_2, ACC binding alone converts ~30% iron sites to five-coordinate. The reaction of O_2 with this complex would lead to an uncoupled reaction, which deactivates the enzyme. (5) The role of CO_2 is to stabilize the six-coordinate ACCO/Fe^{II}/ACC complex, thus preventing the inactivation reaction.

Acknowledgment. This research was supported by grants from the National Institutes of Health (GM40392, E.I.S.; GM24689, J.D.L.; and GM33162, L.Q.).

Supporting Information Available: The temperature dependence of the intensity at the low-energy NIR MCD bands for the ACCO/Fe^{II}/ACC, ACCO/Fe^{II}/ACC/CO_2/ascorbate, and ACCO/Fe^{II}/ACC/ascorbate complexes (PDF). This material is available free of charge via the Internet at http://pubs.acs.org.

JA017250F

(34) Zhou, J.; Wendy, K. L.; Bachmann, B. O.; Gunsior, M.; Townsend, C. A.; Solomon, E. I. *J. Am. Chem. Soc.* **2001**, *123*, 7388−7398.

(35) In this context, it is interesting to compare the K_d value obtained from the NIR CD titration and the apparent K_m value obtained from the steady-state kinetics results. Steady-state kinetics studies indicate that substrate ACC binds less tightly when CO_2 is present. Alternatively, our CD titration studies show the opposite behavior ($K_d = 0.5 \pm 0.3$ mM in the presence of CO_2, and $K_d = 3.5 \pm 1.5$ mM in the absence of CO_2). This difference can be explained by the nonproductive binding of ACC to the deactivated enzyme, which leads to apparent tighter binding due to additional binding modes. The more CO_2 present, the less deactivated enzyme and thus lower apparent affinity of ACC.

(36) Holm, R. H.; Kennepohl, P.; Solomon, E. I. *Chem. Rev.* **1996**, *96*, 2239−2314.

(37) Lee, H.-J.; Lloyd, M. D.; Harlos, K.; Clifton, I. J.; Baldwin, J. E.; Schofield, C. J. *J. Mol. Biol.* **2001**, *308*, 931−948.